The inverse scattering problem by an elastic inclusion

Roman Chapko · Drossos Gintides · Leonidas Mindrinos

Abstract In this work we consider the inverse elastic scattering problem by an inclusion in two dimensions. The elastic inclusion is placed in an isotropic homogeneous elastic medium. The inverse problem, using the third Betti's formula (direct method), is equivalent to a system of four integral equations that are non linear with respect to the unknown boundary. Two equations are on the boundary and two on the unit circle where the far-field patterns of the scattered waves lie. We solve iteratively the system of integral equations by linearising only the far-field equations. Numerical results are presented that illustrate the feasibility of the proposed method.

1 Introduction

The inverse scattering problem consists on finding the shape and the location of an obstacle by measuring the scattered wave, close or far from the scatterer. Depending on the kind of illumination (acoustic, electromagnetic or elastic)

R. Chapko
Faculty of Applied Mathematics and Informatics,
Ivan Franko National University of Lviv, Ukraine
E-mail: chapko@lnu.edu.ua

D. Gintides
Department of Mathematics, National Technical University of Athens, Greece
E-mail: dgindi@math.ntua.gr

L. Mindrinos
Computational Science Center, University of Vienna, Austria
E-mail: leonidas.mindrinos@univie.ac.at

and the properties of the obstacle (soft, hard, penetrable or not) one faces different kind of problems regarding the unique solvability of the problem and the numerical scheme for approximating the solution.

In this work we place the obstacle in a two-dimensional homogeneous and isotropic elastic medium and we assume that it is penetrable, a so-called inclusion, with different Lamé parameters from the exterior domain. This scattering problem has been a subject of research for many years in different fields of physics and engineering due its various applications. For example, in non-destructive testing, geophysical exploration and fracture mechanics.

We consider as incident wave an elastic longitudinal or transversal wave which after interacting with the boundary of the medium is split into an interior (transmitted) wave propagating in the inclusion and a scattered wave traveling in the exterior domain. The scattered wave is also decomposed into a longitudinal and a transversal wave with different wavenumbers that behave like spherical waves with different polarizations at infinity.

Before considering the inverse problem, we should have a good knowledge of the direct problem, which is to find the scattered field and its far-field patterns from the knowledge of the obstacle and the incident wave. The direct problem is linear and well posed for smooth obstacles [27]. The inverse problem, we consider here can be seen as a continuation of [9] where the inverse problem was examined for a rigid scatterer and a cavity. The problem of detecting an elastic inclusion has been also considered for given boundary measurements [1,3], using the factorization method [8], the linear sampling method [29,31], a gradient descent method [24,28] or the probing method [17].

Here, we solve this inverse problem by formulating an equivalent system of non-linear integral equations which has to be solved with a regularization iterative scheme due to its ill-posedness. To avoid an inverse crime we consider the direct method (Betti's formula) for the inverse problem and we keep the indirect approach as proposed in [27] for the direct problem. This method was introduced in [22] and then applied in many different problems, see for instance [5,13,14,26,30] for some recent applications.

The boundary integral equation method is used for both theoretical investigation of uniqueness and stability and also for the numerical solution of many scattering problems. This method is preferable to finite difference method or finite element method because it reduces the dimensions of the problem and results to simple numerical schemes with high convergence order. The only drawback is that it results to dense matrices which in combination with the vector nature of the problem could make the algorithm slower. To handle this problem, we keep the number of terms in the approximating polynomial of the radial function of the parametrized boundary low and we avoid the full linearization of the system.

The final system consists of four equations, two on the unknown boundary taking advantage of the boundary conditions and two on the unit circle assuming that we know the far-field pattern of the scattered fields for one or more incident waves. Even though the first two equations are well-posed, because of the equivalence to the system of integral equations for the direct problem, the

last two inherit the ill-posedness of the system due to the smoothness of the far-field operators. Following [2,16] we apply a two-step method for approximating the radial function. The problem we address here is more involved compared to the electrostatic and acoustic cases thus we expect to get at best similar reconstructions. However, the extra information (pair of far-fields in elasticity) allows us to obtain comparable or even better results compared to the simpler cases.

The two-step method reads as follows: First, we consider the well-posed subsystem to obtain the corresponding densities and then we solve the linearized (with respect to the boundary) ill-posed subsystem to update the initial approximation of the radial function. We consider Tikhonov regularization and the normal equations are solved by the conjugate gradient method.

The paper is organized as follows: in Sect. 2 we formulate the problem in two dimensions and in Sect. 3 we present the direct scattering problem, the elastic potential and the equivalent system of integral equations. The inverse problem is stated in Sect. 4 where we construct also the equivalent system of integral equation using the direct method. In Sect. 5 the two-step method for the parametrized form of the system and the necessary Fréchet derivatives of the operators are presented. In the last section, the numerical examples give satisfactory results and demonstrate the applicability of the proposed method.

2 Problem formulation

We consider the scattering of time-harmonic elastic waves by an isotropic and homogeneous elastic inclusion $D_i \subset \mathbb{R}^2$ with smooth boundary Γ described by the Lamé parameters λ_i, μ_i and the constant density ρ_i. The exterior of D_i described by $D_e = \mathbb{R}^2 \setminus \overline{D}_i$ is filled with an isotropic and homogeneous elastic medium with Lamé constants λ_e, μ_e and density ρ_e. Henceforth, $j = i, e$ counts for the interior D_i and the exterior domain D_e, respectively. In addition, we assume that $\lambda_j + \mu_j > 0$, $\mu_j > 0$ and $\rho_j > 0$.

By $\hat{\boldsymbol{\tau}}$ we define the unit tangent vector to Γ and by $\hat{\boldsymbol{n}} = \mathbf{Q} \cdot \hat{\boldsymbol{\tau}}$ the unit normal vector directed on D_e, where $\mathbf{Q}$ denotes the unitary matrix

$$\mathbf{Q} = \begin{pmatrix} 0 & 1 \\ -1 & 0 \end{pmatrix}.$$

The incident field is either a longitudinal plane wave

$$\mathbf{u}_p^{inc}(\mathbf{x}; \hat{\boldsymbol{d}}) = \hat{\boldsymbol{d}}\, e^{\mathrm{i}k_{p,e}\hat{\boldsymbol{d}}\cdot\mathbf{x}},$$

or a transversal plane wave

$$\mathbf{u}_s^{inc}(\mathbf{x}; \hat{\boldsymbol{d}}) = -\mathbf{Q} \cdot \hat{\boldsymbol{d}}\, e^{\mathrm{i}k_{s,e}\hat{\boldsymbol{d}}\cdot\mathbf{x}},$$

where $\hat{\boldsymbol{d}}$ is the propagation vector and the wavenumbers are given by

$$k_{p,j}^2 := \frac{\rho_j \omega^2}{\lambda_j + 2\mu_j}, \quad k_{s,j}^2 := \frac{\rho_j \omega^2}{\mu_j},$$

where $\omega > 0$ is the circular frequency. In the following, $\alpha = p, s$ counts for the longitudinal and the transversal waves, respectively.

The scattering of $\mathbf{u}^{inc}$ by the inclusion generates the scattered field $\mathbf{u}^e, \mathbf{x} \in D_e$ and the transmitted field $\mathbf{u}^i, \mathbf{x} \in D_i$. Both of them satisfy the Navier equation in their domains of definition

$$\boldsymbol{\Delta}_j^* \mathbf{u}^j + \rho_j \omega^2 \mathbf{u}^j = \mathbf{0}, \quad \text{in } D_j, \tag{1}$$

with the Lamé operator defined by $\boldsymbol{\Delta}_j^* := \mu_j \boldsymbol{\Delta}_j + (\lambda_j + \mu_j) \boldsymbol{\nabla}\boldsymbol{\nabla} \cdot$. If $\mathbf{u}^j$ satisfies (1), due to the Helmholtz decomposition, it can be written as a sum of a longitudinal and a transversal wave

$$\mathbf{u}^j = \mathbf{u}_p^j + \mathbf{u}_s^j,$$

which are defined by

$$\mathbf{u}_p^j := -\frac{1}{k_{p,j}^2} \boldsymbol{\nabla}\boldsymbol{\nabla} \cdot \mathbf{u}^j, \quad \mathbf{u}_s^j := \mathbf{u}^j - \mathbf{u}_p^j.$$

On the boundary we impose transmission conditions of the form

$$\mathbf{u}^i = \mathbf{u}^e + \mathbf{u}^{inc}, \qquad \text{on } \Gamma, \tag{2a}$$

$$\mathbf{T}^i \mathbf{u}^i = \mathbf{T}^e (\mathbf{u}^e + \mathbf{u}^{inc}), \quad \text{on } \Gamma, \tag{2b}$$

where the boundary traction operator $\mathbf{T}^j$ is given by

$$\mathbf{T}^j \mathbf{u}^j := \lambda_j \hat{\boldsymbol{n}} (\boldsymbol{\nabla} \cdot \mathbf{u}^j) + 2\mu_j \left(\hat{\boldsymbol{n}} \cdot \boldsymbol{\nabla} \right) \mathbf{u}^j + \mu_j (\mathbf{Q} \cdot \hat{\boldsymbol{n}}) \boldsymbol{\nabla} \cdot \left(\mathbf{Q} \cdot \mathbf{u}^j \right).$$

The field $\mathbf{u}^e$ is required to satisfy also the Kupradze radiation condition

$$\lim_{r \to \infty} \sqrt{r} \left(\frac{\partial \mathbf{u}_\alpha^e}{\partial r} - i k_{\alpha,e} \mathbf{u}_\alpha^e \right) = \mathbf{0}, \quad r = |\mathbf{x}|, \tag{3}$$

uniformly in all directions. Then, the direct elastic scattering problem reads: Given D_j (geometry and elastic parameters) and the incident field $\mathbf{u}_\alpha^{inc}$, solve the boundary value problem (1) - (3) to obtain $\mathbf{u}^j$.

At this point we recall that any solution of (1) satisfying (3) has an asymptotic behaviour of the form

$$\mathbf{u}_\alpha^e = \frac{e^{ik_{\alpha,e}r}}{\sqrt{r}} \left\{ \mathbf{u}_\alpha^\infty(\hat{\boldsymbol{x}}) + \mathcal{O}\left(\frac{1}{r}\right) \right\}, \quad r \to \infty,$$

uniformly in all directions $\hat{\boldsymbol{x}} = \mathbf{x}/r \in S$, where S denotes the unit circle. The pair $(\mathbf{u}_p^\infty, \mathbf{u}_s^\infty)$ is called the far-field patterns of the scattered field $\mathbf{u}^e$.

3 The direct elastic scattering problem

To represent the solution of the direct and the inverse problem as a combination of an elastic single- and a double-layer potential we first introduce the fundamental solution of the Navier equation

$$\boldsymbol{\Phi}_j(\mathbf{x}, \mathbf{y}) = \frac{\mathrm{i}}{4\mu_j} H_0^{(1)}(k_{s,j} |\mathbf{x} - \mathbf{y}|)\mathbf{I}$$
$$+ \frac{\mathrm{i}}{4\rho_j\omega^2} \boldsymbol{\nabla}\boldsymbol{\nabla}^\top \left[H_0^{(1)}(k_{s,j} |\mathbf{x} - \mathbf{y}|) - H_0^{(1)}(k_{p,j} |\mathbf{x} - \mathbf{y}|) \right]$$

in terms of the the identity matrix $\mathbf{I}$ and the Hankel function $H_0^{(1)}$ of order zero and of the first kind. The Green's tensor can be transformed into

$$\boldsymbol{\Phi}_j(\mathbf{x}, \mathbf{y}) = \Phi_{1,j}(|\mathbf{x} - \mathbf{y}|)\mathbf{I} + \Phi_{2,j}(|\mathbf{x} - \mathbf{y}|)\mathbf{J}(\mathbf{x} - \mathbf{y}),$$

where the functions $\Phi_{1,j}, \Phi_{2,j} : \mathbb{R} \to \mathbb{C}$ are given by [20]

$$\Phi_{1,j}(t) = \frac{\mathrm{i}}{4\mu_j} H_0^{(1)}(k_{s,j}t) - \frac{\mathrm{i}}{4\rho_j\omega^2 t} \left[k_{s,j} H_1^{(1)}(k_{s,j}t) - k_{p,j} H_1^{(1)}(k_{p,j}t) \right],$$

$$\Phi_{2,j}(t) = \frac{\mathrm{i}}{4\rho_j\omega^2} \left[\frac{2k_{s,j}}{t} H_1^{(1)}(k_{s,j}t) - k_{s,j}^2 H_0^{(1)}(k_{s,j}t) - \frac{2k_{p,j}}{t} H_1^{(1)}(k_{p,j}t) \right.$$
$$\left. + k_{p,j}^2 H_0^{(1)}(k_{p,j}t) \right]$$

with $H_1^{(1)} = -H_0^{(1)\prime}$ and

$$\mathbf{J}(\mathbf{x}) = \frac{\mathbf{x}\mathbf{x}^\top}{|\mathbf{x}|^2}, \quad \mathbf{x} \neq \mathbf{0}$$

in terms of a dyadic product of $\mathbf{x}$ with its transpose $\mathbf{x}^\top$. Then, for the vector density $\boldsymbol{\varphi} \in [C^{0,a}(\Gamma)]^2$, $0 < a \leq 1$, we introduce the elastic single-layer potential

$$(\mathbf{S}_j\boldsymbol{\varphi})(\mathbf{x}) = \int_\Gamma \boldsymbol{\Phi}_j(\mathbf{x}, \mathbf{y}) \cdot \boldsymbol{\varphi}(\mathbf{y})ds(\mathbf{y}), \quad \mathbf{x} \in D_j \backslash \Gamma, \tag{4}$$

and the elastic double-layer potential

$$(\mathbf{D}_j\boldsymbol{\varphi})(\mathbf{x}) = \int_\Gamma \left[\mathbf{T}_y^j\boldsymbol{\Phi}_j(\mathbf{x}, \mathbf{y}) \right]^\top \cdot \boldsymbol{\varphi}(\mathbf{y})ds(\mathbf{y}), \quad \mathbf{x} \in D_j \backslash \Gamma. \tag{5}$$

It is well known that $\mathbf{S}_j$ and $\mathbf{T}_x^j\mathbf{D}_j$ are continuous in $\mathbb{R}^2$ but both $\mathbf{D}_j$ and $\mathbf{T}_x^j\mathbf{S}_j$ satisfy the following jump relations [23]

$$\mathbf{D}_j\boldsymbol{\varphi} = \left(\pm\frac{1}{2}\mathbf{I} + \mathbf{K}_j \right)\boldsymbol{\varphi}, \quad \text{on } \Gamma, \tag{6a}$$

$$\mathbf{T}_x^j\mathbf{S}_j\boldsymbol{\varphi} = \left(\mp\frac{1}{2}\mathbf{I} + \mathbf{L}_j \right)\boldsymbol{\varphi}, \quad \text{on } \Gamma, \tag{6b}$$

$$\mathbf{T}_x^j\mathbf{D}_j\boldsymbol{\varphi} = \mathbf{N}_j\boldsymbol{\varphi}, \quad \text{on } \Gamma, \tag{6c}$$

where the upper (lower) sign corresponds to the limit $\mathbf{x} \to \Gamma$ from D_e (D_i), and the integral operators are defined by

$$(\mathbf{K}_j \boldsymbol{\varphi})(\mathbf{x}) = \int_\Gamma \left[\mathbf{T}_y^j \boldsymbol{\Phi}_j(\mathbf{x}, \mathbf{y}) \right]^\top \cdot \boldsymbol{\varphi}(\mathbf{y}) ds(\mathbf{y}), \qquad \mathbf{x} \in \Gamma, \tag{7a}$$

$$(\mathbf{L}_j \boldsymbol{\varphi})(\mathbf{x}) = \int_\Gamma \mathbf{T}_x^j \boldsymbol{\Phi}_j(\mathbf{x}, \mathbf{y}) \cdot \boldsymbol{\varphi}(\mathbf{y}) ds(\mathbf{y}), \qquad \mathbf{x} \in \Gamma, \tag{7b}$$

$$(\mathbf{N}_j \boldsymbol{\varphi})(\mathbf{x}) = \mathbf{T}_x^j \int_\Gamma \left[\mathbf{T}_y^j \boldsymbol{\Phi}_j(\mathbf{x}, \mathbf{y}) \right]^\top \cdot \boldsymbol{\varphi}(\mathbf{y}) ds(\mathbf{y}), \quad \mathbf{x} \in \Gamma. \tag{7c}$$

All the above integrals are well defined and in particular the operator $\mathbf{S}_j$ for $\mathbf{x} \in \Gamma$ is weakly singular, the operators $\mathbf{K}_j$, $\mathbf{L}_j$ are singular and $\mathbf{N}_j$ admits a hypersingular kernel. From the asymptotic behaviour of the Hankel functions we can compute also the far-field patterns of the single- (4) and double-layer potential (5) [6,20]

$$(\mathbf{S}_\alpha^\infty \boldsymbol{\varphi})(\widehat{\boldsymbol{x}}) = \beta_\alpha \int_\Gamma \mathbf{J}_\alpha(\widehat{\boldsymbol{x}}) \cdot \boldsymbol{\varphi}(\mathbf{y}) \, e^{-\mathrm{i}k_{\alpha,e}\widehat{\boldsymbol{x}}\cdot\mathbf{y}} ds(\mathbf{y}), \qquad \widehat{\boldsymbol{x}} \in S, \tag{8a}$$

$$(\mathbf{D}_\alpha^\infty \boldsymbol{\varphi})(\widehat{\boldsymbol{x}}) = \gamma_\alpha \int_\Gamma \mathbf{J}_\alpha(\widehat{\boldsymbol{x}}) \cdot \mathbf{F}(\widehat{\boldsymbol{x}}, \mathbf{y}) \cdot \boldsymbol{\varphi}(\mathbf{y}) \, e^{-\mathrm{i}k_{\alpha,e}\widehat{\boldsymbol{x}}\cdot\mathbf{y}} ds(\mathbf{y}), \quad \widehat{\boldsymbol{x}} \in S, \tag{8b}$$

with the coefficients

$$\beta_p = \frac{e^{\mathrm{i}\pi/4}}{\lambda_e + 2\mu_e} \frac{1}{\sqrt{8\pi k_{p,e}}}, \quad \beta_s = \frac{e^{\mathrm{i}\pi/4}}{\mu_e} \frac{1}{\sqrt{8\pi k_{s,e}}},$$

$$\gamma_p = \frac{e^{-\mathrm{i}\pi/4}}{\lambda_e + 2\mu_e} \sqrt{\frac{k_{p,e}}{8\pi}}, \qquad \gamma_s = \frac{e^{-\mathrm{i}\pi/4}}{\mu_e} \sqrt{\frac{k_{s,e}}{8\pi}},$$

and the matrices $\mathbf{J}_p(\widehat{\boldsymbol{x}}) = \mathbf{J}(\widehat{\boldsymbol{x}})$, $\mathbf{J}_s(\widehat{\boldsymbol{x}}) = \mathbf{I} - \mathbf{J}(\widehat{\boldsymbol{x}})$ and

$$\mathbf{F}(\widehat{\boldsymbol{x}}, \mathbf{y}) = \lambda_e \widehat{\boldsymbol{x}}\, \widehat{\boldsymbol{n}}(\mathbf{y})^\top + \mu_e \widehat{\boldsymbol{n}}(\mathbf{y})\, \widehat{\boldsymbol{x}}^\top + \mu_e (\widehat{\boldsymbol{n}}(\mathbf{y}) \cdot \widehat{\boldsymbol{x}}) \mathbf{I}.$$

Considering the indirect integral equation method, we search the solution of the direct scattering problem in the form

$$\mathbf{u}^j(\mathbf{x}) = (\mathbf{D}_j \boldsymbol{\varphi}_j)(\mathbf{x}) + (\mathbf{S}_j \boldsymbol{\psi}_j)(\mathbf{x}), \quad \mathbf{x} \in D_j. \tag{9}$$

To simplify the above representation, we set

$$\boldsymbol{\varphi}_j(\mathbf{x}) = \tau_j \boldsymbol{\varphi}(\mathbf{x}), \quad \boldsymbol{\psi}_j(\mathbf{x}) = \boldsymbol{\psi}(\mathbf{x}), \quad \tau_j = \frac{\lambda_j + 2\mu_j}{\mu_j(\lambda_j + \mu_j)}$$

and the formula (9) is reduced to

$$\mathbf{u}^j(\mathbf{x}) = \tau_j (\mathbf{D}_j \boldsymbol{\varphi})(\mathbf{x}) + (\mathbf{S}_j \boldsymbol{\psi})(\mathbf{x}), \quad \mathbf{x} \in D_j. \tag{10}$$

Using this representation, applying the jump relations (6) we see that the fields given by (9) satisfy the boundary conditions (2) provided the densities $\boldsymbol{\varphi}$, $\boldsymbol{\psi}$ satisfy the system of integral equations

$$\begin{pmatrix} \mathbf{I} + \mathbf{L}_i - \mathbf{L}_e & \tau_i \mathbf{N}_i - \tau_e \mathbf{N}_e \\ \mathbf{S}_i - \mathbf{S}_e & -\frac{\tau_i + \tau_e}{2}\mathbf{I} + \tau_i \mathbf{K}_i - \tau_e \mathbf{K}_e \end{pmatrix} \begin{pmatrix} \boldsymbol{\psi} \\ \boldsymbol{\varphi} \end{pmatrix} = \begin{pmatrix} \mathbf{T}^e \mathbf{u}^{inc}|_\Gamma \\ \mathbf{u}^{inc}|_\Gamma \end{pmatrix}. \tag{11}$$

The following result regarding uniqueness and existence was proved in [27].

Theorem 1 *The system of integral equations* (11) *has precisely one solution* $(\boldsymbol{\varphi}, \boldsymbol{\psi})$, *with* $\boldsymbol{\varphi} \in [C^{1,a}(\Gamma)]^2$ *and* $\boldsymbol{\psi} \in [C^{0,a}(\Gamma)]^2$. *Moreover, the corresponding displacement fields* (10) *solve the direct scattering problem* (1) - (3).

Then, the solution of the direct problem (10) provides us with the far-field pattern $(\mathbf{u}_p^\infty, \mathbf{u}_s^\infty)$ given by

$$\mathbf{u}_\alpha^\infty(\widehat{\boldsymbol{x}}) = \int_\Gamma \mathbf{J}_\alpha(\widehat{\boldsymbol{x}}) \cdot [\tau_e \gamma_\alpha \mathbf{F}(\widehat{\boldsymbol{x}}, \mathbf{y}) \cdot \boldsymbol{\varphi}(\mathbf{y}) + \beta_\alpha \boldsymbol{\psi}(\mathbf{y})] e^{-\mathrm{i}k_{\alpha,e}\widehat{\boldsymbol{x}}\cdot\mathbf{y}} ds(\mathbf{y}), \quad \widehat{\boldsymbol{x}} \in S,$$
(12)

where we have used the asymptotic forms (8) and that $\boldsymbol{\varphi}$, $\boldsymbol{\psi}$ are the solutions of (11).

Remark 1 The choice of τ_j is not random since, as we are going to see later, the combination $\tau_i \mathbf{N}_i - \tau_e \mathbf{N}_e$ turns out to be a weakly singular operator, reducing the hypersingularity of $\mathbf{N}_j$.

For the numerical implementation, we present also different representations of the solutions in order to distinguish from the formulas we will derive later for the solution of the inverse problem, even though, we are going to consider the direct method. We do not consider the solvability of the above systems. Let the solution of the direct problem be given by

$$\mathbf{u}^j(\mathbf{x}) = (\mathbf{S}_j \boldsymbol{\psi}_j)(\mathbf{x}), \quad \mathbf{x} \in D_j.$$
(13)

Then, considering again the jump relations (6) we see that the fields given now by (13) satisfy the boundary conditions (2) provided the densities $\boldsymbol{\psi}_i$, $\boldsymbol{\psi}_e$ satisfy the system of equations

$$\begin{pmatrix} \mathbf{S}_i & -\mathbf{S}_e \\ \frac{1}{2}\mathbf{I} + \mathbf{L}_i & \frac{1}{2}\mathbf{I} - \mathbf{L}_e \end{pmatrix} \begin{pmatrix} \boldsymbol{\psi}_i \\ \boldsymbol{\psi}_e \end{pmatrix} = \begin{pmatrix} \mathbf{u}^{inc}|_\Gamma \\ \mathbf{T}^e \mathbf{u}^{inc}|_\Gamma \end{pmatrix}.$$

In this case, the far-field patterns are given by $\mathbf{u}_\alpha^\infty(\widehat{\boldsymbol{x}}) = (\mathbf{S}_\alpha^\infty \boldsymbol{\psi}_e)(\widehat{\boldsymbol{x}})$. The fields, considering double-layer representations of the form

$$\mathbf{u}^j(\mathbf{x}) = (\mathbf{D}_j \boldsymbol{\psi}_j)(\mathbf{x}), \quad \mathbf{x} \in D_j,$$
(14)

and the jump relations, satisfy the boundary conditions, provided the densities satisfy

$$\begin{pmatrix} -\frac{1}{2}\mathbf{I} + \mathbf{K}_i & -\frac{1}{2}\mathbf{I} - \mathbf{K}_e \\ \mathbf{N}_i & -\mathbf{N}_e \end{pmatrix} \begin{pmatrix} \boldsymbol{\psi}_i \\ \boldsymbol{\psi}_e \end{pmatrix} = \begin{pmatrix} \mathbf{u}^{inc}|_\Gamma \\ \mathbf{T}^e \mathbf{u}^{inc}|_\Gamma \end{pmatrix}.$$

Here, we obtain the far-field patterns $\mathbf{u}_\alpha^\infty(\widehat{\boldsymbol{x}}) = (\mathbf{D}_\alpha^\infty \boldsymbol{\psi}_e)(\widehat{\boldsymbol{x}})$.

4 The inverse elastic scattering problem

Now we can state the inverse problem, which reads: Find the shape and the position of the inclusion D_i (i.e. reconstruct the boundary) from the knowledge of the far-field patterns $(\mathbf{u}_p^\infty(\widehat{\boldsymbol{x}}), \mathbf{u}_s^\infty(\widehat{\boldsymbol{x}}))$ for all $\widehat{\boldsymbol{x}} \in S$, for one incident plane wave $\mathbf{u}_\alpha^{inc}$ with direction $\hat{\boldsymbol{d}}$ either longitudinal or transverse. In general, the unique solvability of the inverse problem for one or even for a finite number of incident waves is an open problem. Uniqueness for the transmission problem exists only for infinitely many incident waves [11]. There exist also results for a rigid scatterer, local uniqueness in $\mathbb{R}^2$ [9] and measuring only $\mathbf{u}_s^\infty$ for a transversal incident plane wave and simple geometries in $\mathbb{R}^3$ [12].

4.1 The integral equation method

To solve numerically this problem, we consider the non-linear integral equation method, introduced in [22], but here we apply the direct method in contrast to the forward problem. We recall for $\mathbf{v}, \mathbf{w} \in [C^2(\overline{D}_j)]^2$ the third Betti's formula

$$\int_{D_j} (\mathbf{v} \cdot \boldsymbol{\Delta}_j^* \mathbf{w} - \mathbf{w} \cdot \boldsymbol{\Delta}_j^* \mathbf{v}) d\mathbf{x} = \int_\Gamma (\mathbf{v} \cdot \mathbf{T}^j \mathbf{w} - \mathbf{w} \cdot \mathbf{T}^j \mathbf{v}) ds(\mathbf{x}).$$

Using the definitions (4) and (5), we consider the above formula once for the field $\mathbf{u}^e$ and the tensor $\boldsymbol{\Phi}_e$ in D_e, and then for $\mathbf{u}^{inc}, \boldsymbol{\Phi}_e$ in D_e to obtain

$$\mathbf{u}^e(\mathbf{x}) = (\mathbf{D}_e \mathbf{u}^e)(\mathbf{x}) - (\mathbf{S}_e(\mathbf{T}^e \mathbf{u}^e))(\mathbf{x}), \qquad \mathbf{x} \in D_e, \tag{15a}$$

$$\mathbf{0} = (\mathbf{D}_e \mathbf{u}^{inc})(\mathbf{x}) - (\mathbf{S}_e(\mathbf{T}^e \mathbf{u}^{inc}))(\mathbf{x}), \quad \mathbf{x} \in D_e. \tag{15b}$$

We define $\mathbf{u}^t := \mathbf{u}^e + \mathbf{u}^{inc}$ and by adding (15a) and (15b) we obtain

$$\mathbf{u}^e(\mathbf{x}) = (\mathbf{D}_e \mathbf{u}^t)(\mathbf{x}) - (\mathbf{S}_e(\mathbf{T}^e \mathbf{u}^t))(\mathbf{x}), \quad \mathbf{x} \in D_e. \tag{16}$$

Similarly, for $\mathbf{u}^i, \boldsymbol{\Phi}_i$ in D_i, the third Betti's formula results to

$$-\mathbf{u}^i(\mathbf{x}) = (\mathbf{D}_i \mathbf{u}^i)(\mathbf{x}) - (\mathbf{S}_i(\mathbf{T}^i \mathbf{u}^i))(\mathbf{x})$$

$$= (\mathbf{D}_i \mathbf{u}^t)(\mathbf{x}) - (\mathbf{S}_i(\mathbf{T}^e \mathbf{u}^t))(\mathbf{x}), \quad \mathbf{x} \in D_i, \tag{17}$$

where for the last equality we have used the transmission conditions (2). We set $\boldsymbol{\kappa} = \mathbf{u}^t|_\Gamma$ and $\boldsymbol{\mu} = \mathbf{T}^e \mathbf{u}^t|_\Gamma$ and letting $\mathbf{x} \to \Gamma$ in the above representations, taking the traction and considering the jump relations (6), we get

$$\mathbf{u}^j(\mathbf{x}) = (\tfrac{1}{2}\mathbf{I} \pm \mathbf{K}_j)\boldsymbol{\kappa}(\mathbf{x}) \mp (\mathbf{S}_j \boldsymbol{\mu})(\mathbf{x}), \qquad \mathbf{x} \in \Gamma,$$

$$\mathbf{T}^j \mathbf{u}^j(\mathbf{x}) = \pm(\mathbf{N}_j \boldsymbol{\kappa})(\mathbf{x}) + (\tfrac{1}{2}\mathbf{I} \mp \mathbf{L}_j)\boldsymbol{\mu}(\mathbf{x}), \quad \mathbf{x} \in \Gamma.$$

We consider (2) to obtain

$$(\tfrac{1}{2}\mathbf{I} - \mathbf{K}_e)\boldsymbol{\kappa} + \mathbf{S}_e \boldsymbol{\mu} = \mathbf{u}^{inc}, \qquad \text{on } \Gamma, \tag{19a}$$

$$(\tfrac{1}{2}\mathbf{I} + \mathbf{K}_i)\boldsymbol{\kappa} - \mathbf{S}_i \boldsymbol{\mu} = \mathbf{0}, \qquad \text{on } \Gamma, \tag{19b}$$

$$-\mathbf{N}_e\boldsymbol{\kappa} + (\tfrac{1}{2}\mathbf{I} + \mathbf{L}_e)\boldsymbol{\mu} = \mathbf{T}^e\mathbf{u}^{inc}, \quad \text{on } \Gamma, \tag{19c}$$

$$\mathbf{N}_i\boldsymbol{\kappa} + (\tfrac{1}{2}\mathbf{I} - \mathbf{L}_i)\boldsymbol{\mu} = \mathbf{0}, \qquad \text{on } \Gamma. \tag{19d}$$

In addition, given the far-field operators (8) and the representation (16) of the exterior field we observe that the unknown boundary Γ and the densities satisfy the (far-field) equation

$$\begin{pmatrix}\mathbf{D}_p^\infty \\ \mathbf{D}_s^\infty\end{pmatrix}\boldsymbol{\kappa} - \begin{pmatrix}\mathbf{S}_p^\infty \\ \mathbf{S}_s^\infty\end{pmatrix}\boldsymbol{\mu} = \begin{pmatrix}\mathbf{u}_p^\infty \\ \mathbf{u}_s^\infty\end{pmatrix}, \quad \text{on } S,$$

or in compact form

$$\boldsymbol{\mathcal{D}}^\infty\boldsymbol{\kappa} - \boldsymbol{\mathcal{S}}^\infty\boldsymbol{\mu} = \boldsymbol{\mathcal{U}}^\infty \tag{20}$$

where the right-hand side is the known far-field patterns from the direct problem.

Conversely, if $\Gamma, \boldsymbol{\kappa}$ and $\boldsymbol{\mu}$ satisfy (19) and (20), then Γ solves the inverse problem. The equation (19) guarantees the transmission conditions (2) on Γ and the equation (20) ensures that the scattered field given by (16) has the correct far-field patterns.

We observe that we have six equations (19) and (20) for the three unknowns $\Gamma, \boldsymbol{\kappa}$ and $\boldsymbol{\mu}$. In order to take advantage of the well-posedness of the direct problem, we consider the linear combinations (19a) + (19b) and $\tau_e\cdot$(19c) + $\tau_i\cdot$(19d) for the equations on the boundary and we keep the overdetermined far-field equation. Then, considering all the previous arguments, we state the following theorem as a formal formulation of the inverse problem.

Theorem 2 *Given an incident field $\boldsymbol{u}_\alpha^{inc}$, $\alpha = p$ or s and the far-field patterns $\boldsymbol{\mathcal{U}}^\infty$, for all $\widehat{\boldsymbol{x}} \in S$, if Γ and the vector densities $\boldsymbol{\kappa}, \boldsymbol{\mu}$ satisfy the system of integral equations*

$$(\boldsymbol{I} + \boldsymbol{K}_i - \boldsymbol{K}_e)\boldsymbol{\kappa} + (\boldsymbol{S}_e - \boldsymbol{S}_i)\boldsymbol{\mu} = \boldsymbol{u}^{inc}|_\Gamma, \tag{21a}$$

$$(\tau_i\boldsymbol{N}_i - \tau_e\boldsymbol{N}_e)\boldsymbol{\kappa} + (\tfrac{\tau_i + \tau_e}{2}\boldsymbol{I} + \tau_e\boldsymbol{L}_e - \tau_i\boldsymbol{L}_i)\boldsymbol{\mu} = \tau_e\boldsymbol{T}^e\boldsymbol{u}^{inc}|_\Gamma, \tag{21b}$$

$$\boldsymbol{\mathcal{D}}^\infty\boldsymbol{\kappa} - \boldsymbol{\mathcal{S}}^\infty\boldsymbol{\mu} = \boldsymbol{\mathcal{U}}^\infty, \tag{21c}$$

then, Γ solves the inverse problem.

The integral operators involved in (21) are linear with respect to the densities but non-linear with respect to the boundary Γ. The subsystem (21a) - (21b) is equivalent to (11), thus well-posed as already proved [27]. The ill-posedness of the inverse problem is then due to the smooth kernels of the far-field operators in (21c).

In general, there exist three different iterative methods for solving the system (21) by linearization:

A. Given initial guesses for the boundary and the densities, we linearize all three equations in order to update all the unknowns.

B. Given initial guess for the boundary, we solve the subsystem (21a) - (21b) to obtain the densities. Then, keeping the densities fixed we solve the linearized equation (21c) to obtain the update for the boundary.

C. Given initial guesses for the densities, we solve the far-field equation (21c) to obtain Γ and then we solve the linearized form of (21a) - (21b) to obtain the densities.

The linearization, using Fréchet derivatives of the operators, and the regularization of the ill-posed equations are needed in all methods. However, the iterative method A requires the calculation of the Fréchet derivatives of the operators with respect to all unknowns and the selection of two regularization parameters at every step. Thus, we prefer to use one of the so-called two-step methods B or C. Between the two methods, it is obvious that the second method is preferable since we solve first a well-posed linear system and then we linearize only the far-field operators (operators with smooth and simple kernels). From now on, we focus on Method B, a method introduced in [16] and then applied in different problems, see for instance [2,25] for some recent applications.

5 The two-step method

To analyse further the Method B, we consider the following parametrization of the boundary

$$\Gamma = \{\mathbf{z}(t) = r(t)(\cos t,\, \sin t) : t \in [0, 2\pi]\},$$

where $\mathbf{z} : \mathbb{R} \to \mathbb{R}^2$ is a C^2-smooth, 2π-periodic parametrization. We assume in addition that $\mathbf{z}$ is injective in $[0, 2\pi)$, that is $\mathbf{z}'(t) \neq 0$, for all $t \in [0, 2\pi]$. The non-negative function r represents the radial distance of Γ from the origin. Then, we define

$$\boldsymbol{\xi}(t) = \boldsymbol{\kappa}(\mathbf{z}(t)), \quad \boldsymbol{\zeta}(t) = \boldsymbol{\mu}(\mathbf{z}(t)), \quad t \in [0, 2\pi]$$

and the parametrized form of (21) is given by

$$\boldsymbol{\mathcal{A}}(r; \boldsymbol{\xi}) + \boldsymbol{\mathcal{B}}(r; \boldsymbol{\zeta}) = \boldsymbol{\mathcal{C}}, \tag{22}$$

where

$$\boldsymbol{\mathcal{A}} = \begin{pmatrix} \boldsymbol{\mathcal{A}}_1 \\ \boldsymbol{\mathcal{A}}_2 \\ \boldsymbol{\mathcal{A}}_3 \end{pmatrix}, \quad \boldsymbol{\mathcal{B}} = \begin{pmatrix} \boldsymbol{\mathcal{B}}_1 \\ \boldsymbol{\mathcal{B}}_2 \\ \boldsymbol{\mathcal{B}}_3 \end{pmatrix}, \quad \boldsymbol{\mathcal{C}} = \begin{pmatrix} \boldsymbol{\mathcal{C}}_1 \\ \boldsymbol{\mathcal{C}}_2 \\ \boldsymbol{\mathcal{C}}_3 \end{pmatrix},$$

with the parametrized operators

$$(\boldsymbol{\mathcal{A}}_1(r; \boldsymbol{\xi}))(t) = \boldsymbol{\xi}(t) + \int_0^{2\pi} \left[\mathbf{T}^i_{\mathbf{z}(\tau)} \boldsymbol{\Phi}_i(t, \tau) - \mathbf{T}^e_{\mathbf{z}(\tau)} \boldsymbol{\Phi}_e(t, \tau) \right]^\top \cdot \boldsymbol{\xi}(\tau) |\mathbf{z}'(\tau)| d\tau,$$

$$(\boldsymbol{\mathcal{A}}_2(r; \boldsymbol{\xi}))(t) = \int_0^{2\pi} \left(\tau_i \mathbf{T}^i_{\mathbf{z}(t)} \left[\mathbf{T}^i_{\mathbf{z}(\tau)} \boldsymbol{\Phi}_i(t, \tau) \right]^\top \right.$$

$$- \tau_e \mathbf{T}^e_{\mathbf{z}(t)} \left[\mathbf{T}^e_{\mathbf{z}(\tau)} \boldsymbol{\Phi}_e(t,\tau) \right]^\top \right) \cdot \boldsymbol{\xi}(\tau) |\mathbf{z}'(\tau)| d\tau,$$

$$(\boldsymbol{\mathcal{A}}_3(r; \boldsymbol{\xi}))(t) = (\boldsymbol{\mathcal{D}}^\infty(r; \boldsymbol{\xi}))(t),$$

$$(\boldsymbol{\mathcal{B}}_1(r; \boldsymbol{\zeta}))(t) = \int_0^{2\pi} [\boldsymbol{\Phi}_e(t,\tau) - \boldsymbol{\Phi}_i(t,\tau)] \cdot \boldsymbol{\zeta}(\tau) |\mathbf{z}'(\tau)| d\tau,$$

$$(\boldsymbol{\mathcal{B}}_2(r; \boldsymbol{\zeta}))(t) = \frac{\tau_i + \tau_e}{2} \boldsymbol{\zeta}(t)$$
$$+ \int_0^{2\pi} \left(\tau_e \mathbf{T}^e_{\mathbf{z}(t)} \boldsymbol{\Phi}_e(t,\tau) - \tau_i \mathbf{T}^i_{\mathbf{z}(t)} \boldsymbol{\Phi}_i(t,\tau) \right) \cdot \boldsymbol{\zeta}(\tau) |\mathbf{z}'(\tau)| d\tau,$$

$$(\boldsymbol{\mathcal{B}}_3(r; \boldsymbol{\zeta}))(t) = -(\boldsymbol{\mathcal{S}}^\infty(r; \boldsymbol{\zeta}))(t),$$

where $\boldsymbol{\Phi}_j(t,\tau) := \boldsymbol{\Phi}_j(\mathbf{z}(t), \mathbf{z}(\tau))$,

$$(\mathbf{D}^\infty_\alpha(r; \boldsymbol{\xi}))(t) = \gamma_\alpha \int_0^{2\pi} \mathbf{J}_\alpha(\widehat{\boldsymbol{x}}(t)) \cdot \mathbf{F}(\widehat{\boldsymbol{x}}(t), \mathbf{z}(\tau)) \cdot \boldsymbol{\xi}(\tau) \, e^{-\mathrm{i}k_{\alpha,e}\widehat{\boldsymbol{x}}(t) \cdot \mathbf{z}(\tau)} |\mathbf{z}'(\tau)| d\tau,$$

$$(\mathbf{S}^\infty_\alpha(r; \boldsymbol{\zeta}))(t) = \beta_\alpha \int_0^{2\pi} \mathbf{J}_\alpha(\widehat{\boldsymbol{x}}(t)) \cdot \boldsymbol{\zeta}(\tau) \, e^{-\mathrm{i}k_{\alpha,e}\widehat{\boldsymbol{x}}(t) \cdot \mathbf{z}(\tau)} |\mathbf{z}'(\tau)| d\tau$$

and the right-hand side

$$(\boldsymbol{\mathcal{C}}_1(r))(t) = \mathbf{u}^{inc}(\mathbf{z}(t)), \quad (\boldsymbol{\mathcal{C}}_2(r))(t) = \tau_e (\mathbf{T}^e \mathbf{u}^{inc})(\mathbf{z}(t)), \quad \boldsymbol{\mathcal{C}}_3(t) = \boldsymbol{\mathcal{U}}^\infty(\widehat{\boldsymbol{x}}(t)).$$

Remark 2 The operators $\boldsymbol{\mathcal{A}}_k$, $\boldsymbol{\mathcal{B}}_k$, $k = 1, 2, 3$ act on the densities and the first variable r shows the dependence on the unknown parametrization of the boundary. Only $\boldsymbol{\mathcal{C}}_3$ is independent of the radial function.

The two-step method for the system (22) reads as follows:

Iterative Scheme 1 *Initially, we give an approximation of the radial function $r^{(0)}$. Then, in the kth iteration step:*

i. *We assume that we know $r^{(k-1)}$ and we solve the subsystem*

$$\binom{\boldsymbol{\mathcal{A}}_1}{\boldsymbol{\mathcal{A}}_2} (r^{(k-1)}; \boldsymbol{\xi}) + \binom{\boldsymbol{\mathcal{B}}_1}{\boldsymbol{\mathcal{B}}_2} (r^{(k-1)}; \boldsymbol{\zeta}) = \binom{\boldsymbol{\mathcal{C}}_1}{\boldsymbol{\mathcal{C}}_2} (r^{(k-1)}), \qquad (23)$$

to obtain the densities $\boldsymbol{\xi}^{(k)}$, $\boldsymbol{\zeta}^{(k)}$.

ii. *Then, keeping the densities fixed, we linearize the third equation of (22), namely*

$$\boldsymbol{\mathcal{A}}_3(r^{(k-1)}; \boldsymbol{\xi}^{(k)}) + (\boldsymbol{\mathcal{A}}'_3(r^{(k-1)}; \boldsymbol{\xi}^{(k)}))(q) + \boldsymbol{\mathcal{B}}_3(r^{(k-1)}; \boldsymbol{\zeta}^{(k)})$$
$$+ (\boldsymbol{\mathcal{B}}'_3(r^{(k-1)}; \boldsymbol{\zeta}^{(k)})(q) = \boldsymbol{\mathcal{C}}_3. \quad (24)$$

We solve this equation for q and we update the radial function $r^{(k)} = r^{(k-1)} + q$.

The iteration stops when a suitable stopping criterion is satisfied.

The function q stands for the radial function of the perturbed boundary

$$\Gamma_q = \{\mathbf{q}(t) = q(t)(\cos t,\, \sin t) : t \in [0, 2\pi]\},$$

and the Fréchet derivatives of the operators are calculated by formally differentiating their kernels with respect to r [7]

$$(\boldsymbol{\mathcal{A}}_3'(r; \boldsymbol{\xi}))(q) = \begin{pmatrix} (\mathbf{D}_p^{\infty\,\prime}(r; \boldsymbol{\xi}))(q) \\ (\mathbf{D}_s^{\infty\,\prime}(r; \boldsymbol{\xi}))(q) \end{pmatrix}, \quad (\boldsymbol{\mathcal{B}}_3'(r; \boldsymbol{\zeta}))(q) = - \begin{pmatrix} (\mathbf{S}_p^{\infty\,\prime}(r; \boldsymbol{\zeta}))(q) \\ (\mathbf{S}_s^{\infty\,\prime}(r; \boldsymbol{\zeta}))(q) \end{pmatrix}$$

with

$$((\mathbf{D}_\alpha^{\infty\,\prime}(r; \boldsymbol{\xi}))(q))(t) = \gamma_\alpha \int_0^{2\pi} \mathbf{J}_\alpha(\widehat{\boldsymbol{x}}(t)) \cdot \mathbf{G}_\alpha(t, \tau) \cdot \boldsymbol{\xi}(\tau)\, e^{-\mathrm{i}k_{\alpha,e}\widehat{\boldsymbol{x}}(t) \cdot \mathbf{z}(\tau)} d\tau,$$

$$((\mathbf{S}_\alpha^{\infty\,\prime}(r; \boldsymbol{\zeta}))(q))(t) = \beta_\alpha \int_0^{2\pi} g_\alpha(t, \tau) \mathbf{J}_\alpha(\widehat{\boldsymbol{x}}(t)) \cdot \boldsymbol{\zeta}(\tau)\, e^{-\mathrm{i}k_{\alpha,e}\widehat{\boldsymbol{x}}(t) \cdot \mathbf{z}(\tau)} d\tau,$$

where $\mathbf{G}_\alpha(t, \tau) := \mathbf{G}_\alpha(\widehat{\boldsymbol{x}}(t), \mathbf{z}(\tau), \mathbf{q}(\tau))$ with

$$\mathbf{G}_\alpha(\widehat{\boldsymbol{x}}(t), \mathbf{z}(\tau), \mathbf{q}(\tau)) = \lambda_e \widehat{\boldsymbol{x}}(t)\mathbf{v}(\tau)^\top + \mu_e \mathbf{v}(\tau)\widehat{\boldsymbol{x}}(t)^\top + \mu_e(\mathbf{v}(\tau) \cdot \widehat{\boldsymbol{x}}(t))\mathbf{I}$$
$$- \mathrm{i}k_{\alpha,e}(\widehat{\boldsymbol{x}}(t) \cdot \mathbf{q}(\tau))\,|\mathbf{z}'(\tau)|\,\mathbf{F}(\widehat{\boldsymbol{x}}(t), \mathbf{z}(\tau))$$

for $\mathbf{v}(\tau) := \mathbf{Q} \cdot \mathbf{q}'(\tau)$ and $g_\alpha(t, \tau) := g_\alpha(\widehat{\boldsymbol{x}}(t), \mathbf{z}(\tau), \mathbf{q}(\tau))$ with

$$g_\alpha(\widehat{\boldsymbol{x}}(t), \mathbf{z}(\tau), \mathbf{q}(\tau)) = -\mathrm{i}k_{\alpha,e}(\widehat{\boldsymbol{x}}(t) \cdot \mathbf{q}(\tau))\,|\mathbf{z}'(\tau)| + \frac{\mathbf{z}'(\tau) \cdot \mathbf{q}'(\tau)}{|\mathbf{z}'(\tau)|}.$$

To show injectivity of the integral operators involved in (24), we consider a simplified linearization. Assuming that $\mathbf{z}'$ is known, we linearize with respect to $\mathbf{z}$ only, viewing $\mathbf{z}'$ as independent of $\mathbf{z}$, resulting to

$$((\mathbf{D}_\alpha^{\infty\,\prime}(r; \boldsymbol{\xi}))(q))(t) = -\mathrm{i}k_{\alpha,e}\gamma_\alpha \int_0^{2\pi} (\widehat{\boldsymbol{x}}(t) \cdot \mathbf{q}(\tau))\mathbf{J}_\alpha(\widehat{\boldsymbol{x}}(t)) \cdot \mathbf{F}(\widehat{\boldsymbol{x}}(t), \mathbf{z}(\tau))$$
$$\cdot \boldsymbol{\xi}(\tau) e^{-\mathrm{i}k_{\alpha,e}\widehat{\boldsymbol{x}}(t) \cdot \mathbf{z}(\tau)} d\tau,$$

$$((\mathbf{S}_\alpha^{\infty\,\prime}(r; \boldsymbol{\zeta}))(q))(t) = -\mathrm{i}k_{\alpha,e}\beta_\alpha \int_0^{2\pi} (\widehat{\boldsymbol{x}}(t) \cdot \mathbf{q}(\tau))\mathbf{J}_\alpha(\widehat{\boldsymbol{x}}(t))$$
$$\cdot \boldsymbol{\zeta}(\tau)\, e^{-\mathrm{i}k_{\alpha,e}\widehat{\boldsymbol{x}}(t) \cdot \mathbf{z}(\tau)} d\tau,$$

where now $\boldsymbol{\xi}(\tau) := \boldsymbol{\xi}(\tau)\,|\mathbf{z}'(\tau)|$ and $\boldsymbol{\zeta}(\tau) := \boldsymbol{\zeta}(\tau)\,|\mathbf{z}'(\tau)|$. In addition, we recall that for sufficiently small q, the perturbed boundary Γ_q can be represented by $\mathbf{q}(t) = \tilde{q}(t)\mathbf{Q} \cdot \mathbf{z}'(t)$, $t \in [0, 2\pi]$ [15]. Now we can state the following theorem considering the above formulas for the Fréchet derivatives and as unknown the function $\tilde{q}$.

Theorem 3 *Let $\boldsymbol{\xi}, \boldsymbol{\zeta}$ solve (23) and let r be the radial function of the unperturbed boundary Γ. If $\tilde{q} \in C^2[0, 2\pi]$ satisfies the homogeneous form of equation (24), meaning*

$$(\boldsymbol{\mathcal{A}}_3'(r; \boldsymbol{\xi}) + \boldsymbol{\mathcal{B}}_3'(r; \boldsymbol{\zeta}))(\tilde{q}) = 0, \tag{25}$$

then $\tilde{q} = 0$.

Proof We follow the ideas presented in [15] for the Laplace operator. Equation (25) is equivalent to

$$(\mathbf{D}_\alpha^{\infty}{}'(r;\boldsymbol{\xi}) - \mathbf{S}_\alpha^{\infty}{}'(r;\boldsymbol{\zeta}))(\tilde{q}) = 0, \quad \alpha = p, s. \tag{26}$$

We introduce the function

$$V(\mathbf{x}) = \int_0^{2\pi} \frac{\partial}{\partial \hat{n}(\mathbf{z}(\tau))} \left[\mathbf{T}_{\mathbf{z}(\tau)}^e \boldsymbol{\Phi}_e(\mathbf{x}, \mathbf{z}(\tau)) \right]^\top \cdot \boldsymbol{\xi}(\tau) \tilde{q}(\tau) \, |\mathbf{z}'(\tau)| \, d\tau$$

$$- \int_0^{2\pi} \frac{\partial}{\partial \hat{n}(\mathbf{z}(\tau))} \boldsymbol{\Phi}_e(\mathbf{x}, \mathbf{z}(\tau)) \cdot \boldsymbol{\zeta}(\tau) \tilde{q}(\tau) \, |\mathbf{z}'(\tau)| \, d\tau, \quad \mathbf{x} \in D_e,$$

which is a radiating solution of (1) in D_e. The far-field patterns of V are given by

$$V_\alpha^{\infty}(\widehat{\boldsymbol{x}}) = \int_0^{2\pi} \frac{\partial}{\partial \mathbf{z}(\tau)} \boldsymbol{\Psi}_\alpha^{\infty}(\widehat{\boldsymbol{x}}, \mathbf{z}(\tau)) \cdot \boldsymbol{\xi}(\tau) \tilde{q}(\tau) \, |\mathbf{z}'(\tau)| \, d\tau$$

$$- \int_0^{2\pi} \frac{\partial}{\partial \mathbf{z}(\tau)} \boldsymbol{\Phi}_\alpha^{\infty}(\widehat{\boldsymbol{x}}, \mathbf{z}(\tau)) \cdot \boldsymbol{\zeta}(\tau) \tilde{q}(\tau) \, |\mathbf{z}'(\tau)| \, d\tau, \quad \widehat{\boldsymbol{x}} \in S,$$

where $\boldsymbol{\Psi}_\alpha^{\infty}(\widehat{\boldsymbol{x}}, \mathbf{z}(\tau)) = \gamma_\alpha \mathbf{J}_\alpha(\widehat{\boldsymbol{x}}) \cdot \mathbf{F}(\widehat{\boldsymbol{x}}, \mathbf{z}(\tau)) e^{-\mathrm{i}k_{\alpha,e}\widehat{\boldsymbol{x}}\cdot\mathbf{z}(\tau)}$ and $\boldsymbol{\Phi}_\alpha^{\infty}(\widehat{\boldsymbol{x}}, \mathbf{z}(\tau)) = \beta_\alpha \mathbf{J}_\alpha(\widehat{\boldsymbol{x}}) e^{-\mathrm{i}k_{\alpha,e}\widehat{\boldsymbol{x}}\cdot\mathbf{z}(\tau)}$. We observe that V_α^{∞} coincide with the left hand-side of (26) since also $\mathbf{F}$ is independent of $\mathbf{z}$. Then, $V_\alpha^{\infty} \equiv 0$, and by Rellich's Lemma we get that $V(\mathbf{x}) = 0$, $\mathbf{x} \in D_e$. In this equation the first integral has a hypersingular kernel and the second one a kernel with lower singularity. Since the fundamental solution of the Navier equation has the same (logarithmic) singularity as the fundamental solution of the Laplace equation, we can show that $\boldsymbol{\xi}(t)\tilde{q}(t) = 0$ for almost every $t \in [0, 2\pi]$ [15]. An application of unique continuation and the Holmgren theorem [18] results to $\tilde{q} = 0$, since $\boldsymbol{\xi}$ cannot be zero on Γ.

6 Numerical implementation

In this section we first justify numerically the convergence of the proposed scheme using analytic solutions of the direct problem and then we investigate the applicability of the Iterative Scheme 1 for solving the inverse problem. We solve both integral equations systems using the Nyström method.

To handle the singularities of the kernels we consider the following representations. The kernel of the parametrized operator $\mathbf{S}_j$ admits the decomposition

$$\boldsymbol{\Phi}_j(t, \tau) = \mathbf{K}_{j,1}(t, \tau) \ln\left(4\sin^2\left(\frac{t-\tau}{2}\right)\right) + \mathbf{K}_{j,2}(t, \tau), \tag{27}$$

for smooth kernels $\mathbf{K}_{j,1}, \mathbf{K}_{j,2}$, given for instance in [20]. To compute the kernels $\mathbf{T}_{\mathbf{v}}^j \boldsymbol{\Phi}_j(t, \tau)$, for $\mathbf{v} = \mathbf{z}(t)$, $\mathbf{z}(\tau)$ we consider the differences $\boldsymbol{\Phi}_j - \boldsymbol{\Phi}_j^{(0)}$, where $\boldsymbol{\Phi}_j^{(0)}$

denotes the fundamental solution of the static ($\omega = 0$) Navier equation [6]. Then, we obtain the forms

$$\mathbf{T}_{\mathbf{v}}^{j} \boldsymbol{\Phi}_j(t,\tau) = \mathbf{T}_{\mathbf{v}}^{j} \left(\boldsymbol{\Phi}_j(t,\tau) - \boldsymbol{\Phi}_j^{(0)}(t,\tau) \right) + \mathbf{T}_{\mathbf{v}}^{j} \boldsymbol{\Phi}_j^{(0)}(t,\tau). \qquad (28)$$

The first term on the right-hand side is weakly singular and can be written in the form (27), while the second term due to its Cauchy type singularity is decomposed as follows

$$\mathbf{T}_{\mathbf{v}}^{j} \boldsymbol{\Phi}_j^{(0)}(t,\tau) = \mathbf{L}_{j,1}^{\mathbf{v}}(t,\tau) \ln \left(4 \sin^2 \left(\frac{t-\tau}{2} \right) \right) + \mathbf{L}_{j,2}^{\mathbf{v}}(t,\tau)$$
$$- \mathbf{Q} \frac{\mu_j}{4\pi(\lambda_j + 2\mu_j)} \cot \left(\frac{\tau - t}{2} \right)$$

where $\mathbf{L}_{j,1}^{\mathbf{v}}, \mathbf{L}_{j,2}^{\mathbf{v}}$ are smooth kernels, for $\mathbf{v} = \mathbf{z}(t), \mathbf{z}(\tau)$. The kernel of the operator $\tau_i \mathbf{N}_i - \tau_e \mathbf{N}_e$ appearing in (11) and in $\mathcal{A}_2$, consists of two hypersingular terms but it turns out to be weakly singular, as discussed in Remark 1. As in (28), we consider the following decomposition

$$\mathbf{T}_{\mathbf{z}(t)}^{j} \left[\mathbf{T}_{\mathbf{z}(\tau)}^{j} \boldsymbol{\Phi}_j(t,\tau) \right]^{\top} = \mathbf{T}_{\mathbf{z}(t)}^{j} \left[\mathbf{T}_{\mathbf{z}(\tau)}^{j} \left(\boldsymbol{\Phi}_j(t,\tau) - \boldsymbol{\Phi}_j^{(0)}(t,\tau) \right) \right]^{\top}$$
$$+ \mathbf{T}_{\mathbf{z}(t)}^{j} \left[\mathbf{T}_{\mathbf{z}(\tau)}^{j} \boldsymbol{\Phi}_j^{(0)}(t,\tau) \right]^{\top}, \qquad (29)$$

The first term is weakly singular and the second one preserves the hypersingularity. The advantage, of this decomposition, is that the second term coming from the static case is easier to handle by a Maue-type expression [6], although it is not needed here. The integral operator with kernel the second term can be written as [4, Equation 2.6]

$$(\mathbf{N}_j^{(0)}(r; \boldsymbol{\xi}))(t) = \int_0^{2\pi} \mathbf{T}_{\mathbf{z}(t)}^{j} \left[\mathbf{T}_{\mathbf{z}(\tau)}^{j} \boldsymbol{\Phi}_j^{(0)}(t,\tau) \right]^{\top} \cdot \boldsymbol{\xi}(\tau) |\mathbf{z}'(\tau)| d\tau$$
$$= \frac{c_j}{2\pi |\mathbf{z}'(t)|} \int_0^{2\pi} \left[\cot \frac{\tau - t}{2} \boldsymbol{\xi}'(\tau) + \mathbf{K}(t,\tau) \cdot \boldsymbol{\xi}(\tau) \right] d\tau,$$

for a smooth kernel $\mathbf{K}$ independent of D_j and $c_j = \mu_j(\lambda_j + \mu_j)/(\lambda_j + 2\mu_j)$. Since $c_j = \tau_j^{-1}$, we see that

$$\tau_i (\mathbf{N}_i^{(0)}(r; \boldsymbol{\xi}))(t) - \tau_e (\mathbf{N}_e^{(0)}(r; \boldsymbol{\xi}))(t) = 0.$$

Then, the combination $\tau_i \mathbf{N}_i - \tau_e \mathbf{N}_e$ presents only weakly singularity due to the first term in (29).

We consider $2n$ equidistant nodal points $t_j = j\pi/n$, $j = 0, ..., 2n - 1$ and we use the trapezoidal rule to approximate the operators with smooth kernels

$$\int_0^{2\pi} \boldsymbol{\xi}(\tau) d\tau \approx \frac{\pi}{n} \sum_{j=0}^{2n-1} \boldsymbol{\xi}(t_j),$$

and the following quadrature rules for the singular kernels [19,21]

$$\int_0^{2\pi} \ln\left(4\sin^2\left(\frac{t-\tau}{2}\right)\right) \boldsymbol{\xi}(\tau) d\tau \approx \sum_{j=0}^{2n-1} R_j^{(n)}(t)\boldsymbol{\xi}(t_j),$$

$$\frac{1}{4\pi}\int_0^{2\pi} \cot\left(\frac{\tau-t}{2}\right) \boldsymbol{\xi}'(\tau) d\tau \approx \sum_{j=0}^{2n-1} T_j^{(n)}(t)\boldsymbol{\xi}(t_j),$$

$$\int_0^{2\pi} \cot\left(\frac{\tau-t}{2}\right) \boldsymbol{\xi}(\tau) d\tau \approx \sum_{j=0}^{2n-1} S_j^{(n)}(t)\boldsymbol{\xi}(t_j),$$

with weights

$$R_j^{(n)}(t) = -\frac{2\pi}{n}\sum_{m=1}^{n-1} \frac{1}{m}\cos\left(m(t-t_j)\right) - \frac{\pi}{n^2}\cos(n(t-t_j)),$$

$$T_j^{(n)}(t) = -\frac{1}{2n}\sum_{m=1}^{n-1} m\cos\left(m(t-t_j)\right) - \frac{1}{4}\cos(n(t-t_j)),$$

$$S_j^{(n)}(t) = \frac{\pi}{n}\left[1-(-1)^j\cos(nt)\right]\cot\left(\frac{t_j-t}{2}\right), \quad t \neq t_j.$$

The error and convergence analysis of the proposed numerical method can be carried out based on the theory of operator approximations and on estimates for trigonometrical interpolation in Sobolev spaces [21, Section 12.4]. This analysis shows that the applied method admits super-algebraic convergence and in the case of analytical data it convergences exponentially.

In the following examples, we consider three different parametrizations of the boundary curves.

A peanut-shaped boundary with radial function

$$r(t) = (0.5\cos^2 t + 0.15\sin^2 t)^{1/2}, \quad t \in [0, 2\pi],$$

an apple-shaped boundary with radial function

$$r(t) = \frac{0.45 + 0.3\cos t - 0.1\sin 2t}{1 + 0.7\cos t}, \quad t \in [0, 2\pi],$$

and a kite-shaped boundary with parametrization

$$\mathbf{z}(t) = (\cos t + 0.7\cos 2t, \ 1.2\sin t), \quad t \in [0, 2\pi].$$

6.1 Example with analytic solution

We consider two arbitrary points $\mathbf{z}_i \in D_i$ and $\mathbf{z}_e \in D_e$ and we define the vector-valued boundary functions

$$\mathbf{f} = [\boldsymbol{\Phi}_i(\mathbf{x}, \mathbf{z}_e)]_1 - [\boldsymbol{\Phi}_e(\mathbf{x}, \mathbf{z}_i)]_1, \qquad \text{on } \Gamma,$$

$$\mathbf{g} = [\mathbf{T}_x^i\boldsymbol{\Phi}_i(\mathbf{x}, \mathbf{z}_e)]_1 - [\mathbf{T}_x^e\boldsymbol{\Phi}_e(\mathbf{x}, \mathbf{z}_i)]_1, \quad \text{on } \Gamma,$$
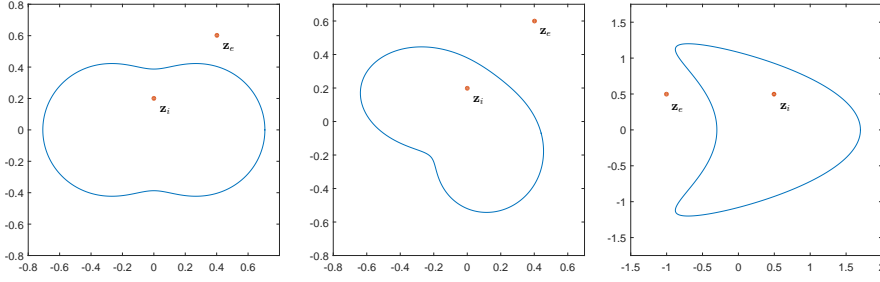
Fig. 1 The source points considered for the different boundary curves.

where $[\cdot]_1$ denotes the first column of the tensor. Then, the fields

$$\mathbf{u}^i(\mathbf{x}) = [\boldsymbol{\Phi}_i(\mathbf{x}, \mathbf{z}_e)]_1, \quad \mathbf{x} \in D_i, \qquad \mathbf{u}^e(\mathbf{x}) = [\boldsymbol{\Phi}_e(\mathbf{x}, \mathbf{z}_i)]_1, \quad \mathbf{x} \in D_e,$$

satisfy the Navier equations (1) and the transmission boundary conditions

$$\mathbf{u}^i = \mathbf{u}^e + \mathbf{f}, \qquad \text{on } \Gamma,$$
$$\mathbf{T}^i \mathbf{u}^i = \mathbf{T}^e \mathbf{u}^e + \mathbf{g}, \quad \text{on } \Gamma.$$

In addition, $\mathbf{u}^e$ satisfies the Kupradze radiation condition (3). The exact values of the far-field patterns of $\mathbf{u}^e$ considering the asymptotic behaviour of the Hankel function are given by

$$\phi_\alpha^\infty(\widehat{\boldsymbol{x}}, \mathbf{z}_i) = \beta_\alpha \, e^{-ik_{\alpha,e}\widehat{\boldsymbol{x}}\cdot\mathbf{z}_i}[\mathbf{J}_\alpha(\widehat{\boldsymbol{x}})]_1, \quad \alpha = p, s.$$

To compute numerically the far-field patterns we consider the three different integral representations of the solution, meaning equations (11), (13) and (14) in order to show the efficiency of the numerical scheme. Then, the densities satisfy the corresponding systems of equations for $\mathbf{f} = \mathbf{u}^{inc}|_\Gamma$ and $\mathbf{g} = \mathbf{T}^e \mathbf{u}^{inc}|_\Gamma$.

n	$\mathbf{u}_{p,1}^\infty(\widehat{\boldsymbol{x}}(0))$	$\mathbf{u}_{p,1}^\infty(\widehat{\boldsymbol{x}}(\pi/4))$
8	$0.021470558670546 + i\,0.022335063461969$	$0.015209469321064 + i\,0.002605280958500$
16	$0.021873642791839 + i\,0.021893613229408$	$0.015342524818313 + i\,0.002060474589649$
32	$0.021876587646542 + i\,0.021876540811223$	$0.015334092161171 + i\,0.002039057704230$
64	$0.021876565329344 + i\,0.021876565329354$	$0.015334087405495 + i\,0.002039073011261$
	$\phi_{p,1}^\infty(\widehat{\boldsymbol{x}}(0))$	$\phi_{p,1}^\infty(\widehat{\boldsymbol{x}}(\pi/4))$
	$0.021876565329347 + i\,0.021876565329347$	$0.015334087405495 + i\,0.002039073011258$

Table 1 The computed and the exact longitudinal far-field for the peanut-shaped boundary considering the representation (10).

n	$\mathbf{u}_{s,2}^{\infty}(\widehat{\boldsymbol{x}}(0))$	$\mathbf{u}_{s,2}^{\infty}(\widehat{\boldsymbol{x}}(\pi/4))$
8	$-0.000799863220578 - \mathrm{i}\,0.002335597090466$	$-0.031580574133787 + \mathrm{i}\,0.015384692677552$
16	$-0.000014894279556 - \mathrm{i}\,0.000022763052245$	$-0.033171141088210 + \mathrm{i}\,0.011955071914825$
32	$-0.000000000009438 - \mathrm{i}\,0.000000000006972$	$-0.033172445082299 + \mathrm{i}\,0.011957712237710$
64	$-0.000000000000002 - \mathrm{i}\,0.000000000000008$	$-0.033172445069954 + \mathrm{i}\,0.011957712196999$
	$\boldsymbol{\phi}_{s,2}^{\infty}(\widehat{\boldsymbol{x}}(0))$	$\boldsymbol{\phi}_{s,2}^{\infty}(\widehat{\boldsymbol{x}}(\pi/4))$
	$0.000000000000000 + \mathrm{i}\,0.000000000000000$	$-0.033172445069954 + \mathrm{i}\,0.011957712197001$

Table 2 The computed and the exact transversal far-field for the apple-shaped boundary considering the representation (14).

n	$\mathbf{u}_{p,1}^{\infty}(\widehat{\boldsymbol{x}}(\pi/4))$	$\mathbf{u}_{s,1}^{\infty}(\widehat{\boldsymbol{x}}(\pi/4))$
16	$-0.010422864908398 - \mathrm{i}\,0.010511643137096$	$0.006390366624901 + \mathrm{i}\,0.055889882020365$
32	$-0.012209281542488 - \mathrm{i}\,0.009493771192078$	$0.005583999436220 + \mathrm{i}\,0.034801431044799$
64	$-0.012210910150120 - \mathrm{i}\,0.009496616688802$	$0.005585376568695 + \mathrm{i}\,0.034816685008179$
128	$-0.012210910180807 - \mathrm{i}\,0.009496616653359$	$0.005585376688542 + \mathrm{i}\,0.034816685082766$
	$\boldsymbol{\phi}_{p,1}^{\infty}(\widehat{\boldsymbol{x}}(\pi/4))$	$\boldsymbol{\phi}_{s,1}^{\infty}(\widehat{\boldsymbol{x}}(\pi/4))$
	$-0.012210910180807 - \mathrm{i}\,0.009496616653360$	$0.005585376688542 + \mathrm{i}\,0.034816685082766$

Table 3 The computed and the exact far-fields for the kite-shaped boundary considering the representation (13).

In all examples we choose the Lamé constants to be $\lambda_e = 1$, $\mu_e = 1$ and $\rho_e = 1$ in D_e and $\lambda_i = 2$, $\mu_i = 2$ and $\rho_i = 1$ in D_i and $\omega = 8$ circular frequency. We consider the source points $\mathbf{z}_i = (0, 0.2)$ and $\mathbf{z}_e = (0.4, 0.6)$ for the peanut-shaped and the apple-shaped boundary and the points $\mathbf{z}_i = (0.5, 0.5)$ and $\mathbf{z}_e = (-1, 0.5)$ for the kite-shaped boundary, see Fig. 1.

In Tables 1, 2 and 3 we present the numerical values of the components of the far-fields patterns at given directions. We obtain the correct values related to the point source located in D_i, combining different representations of the solutions with the boundary parametrizations. This shows that our approach is applicable in all cases. The exponential convergence is clearly exhibited, as we can see also in Fig. 2.

All algorithms were implemented in Matlab 2016b using an Intel Core i7-4820K at 3.70GHz workstation equipped with 64 GB RAM. Even though we deal with dense matrices of size $8n \times 8n$, the computations are considerably fast because of the exponential convergence. The values for $n = 64$ in Tables 1 and 2 were obtained in less than 2.5 and 2 seconds, respectively. The algorithm produces the computed far-fields of Table 3, for $n = 128$ in less than 3 seconds.
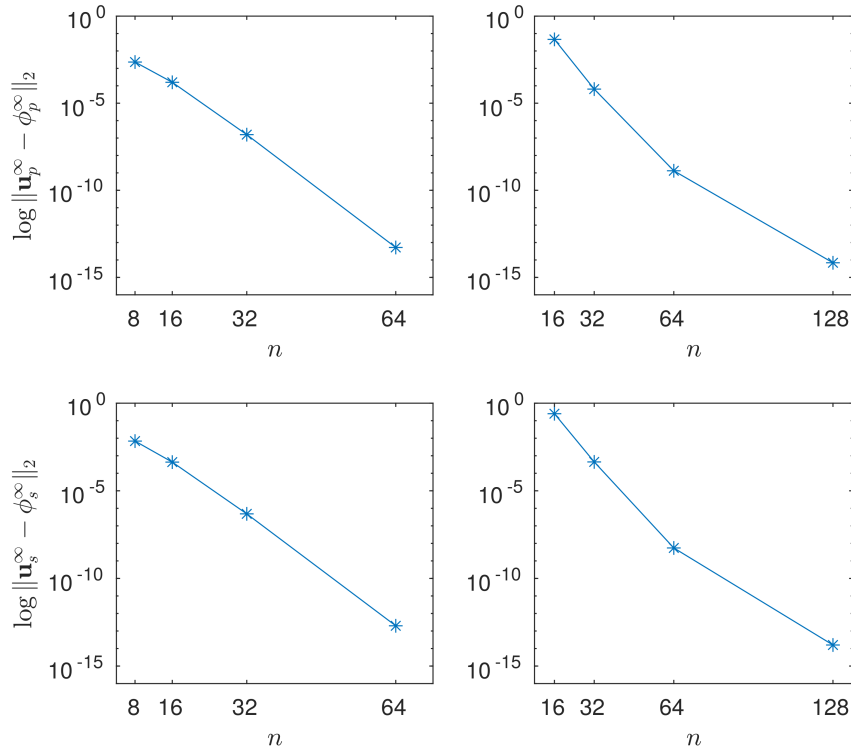
Fig. 2 The L^2 norm (in logarithmic scale) of the difference between the computed and the exact longitudinal (top row) and transversal (bottom row) far-fields. The parameters are the same as in Table 1 (left column) and Table 3 (right column).

6.2 The inverse problem

To avoid an inverse crime in the following examples, the simulated far-field data were obtained by solving numerically the direct problem, replacing (10) by (13) and considering double amount of collocation points.

We approximate the radial function q by a trigonometric polynomial of the form

$$q(t) \approx \sum_{k=0}^{m} a_k \cos kt + \sum_{k=1}^{m} b_k \sin kt, \quad t \in [0, 2\pi].$$

The subsystem (23) is well-posed and no special treatment is required. We solve the ill-posed linearized equation (24) by minimizing the Tikhonov functional of the corresponding discretized equation

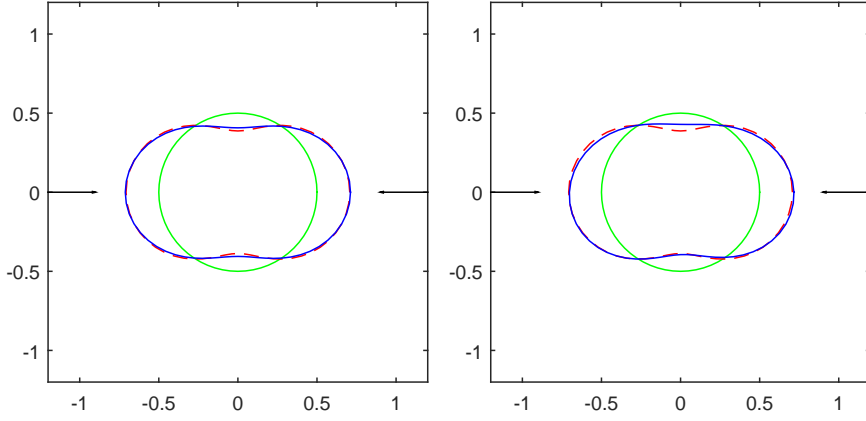$$\|\mathbf{AT}\mathbf{x} - \mathbf{b}\|_2^2 + \lambda \|\mathbf{x}\|_p^p, \quad \lambda > 0.$$

Fig. 3 Reconstruction of a peanut-shaped boundary for exact (left) and noisy (right) data.

where $\mathbf{x} \in \mathbb{R}^{(2m+1)\times 1}$ is the vector with the unknowns coefficients $a_0, ..., a_m$, $b_1, ..., b_m$ of the radial function, and $\mathbf{A} \in \mathbb{C}^{8n\times 8n}$, $\mathbf{b} \in \mathbb{C}^{8n\times 1}$ are given by

$$\mathbf{A}_{kj} = \mathbf{M}_{\mathcal{A}_3'}(t_k, t_j) + \mathbf{M}_{\mathcal{B}_3'}(t_k, t_j),$$
$$\mathbf{b}_k = \mathcal{C}_3(t_k) - (\mathbf{M}_{\mathcal{A}_3} \cdot \boldsymbol{\xi})(t_k) - (\mathbf{M}_{\mathcal{B}_3} \cdot \boldsymbol{\zeta})(t_k),$$

for $k, j = 0, ..., 2n-1$, where $\mathbf{M}_{\mathcal{K}}$ denotes the matrix related to the discretized kernel of the operator $\mathcal{K}$. The multiplication matrix $\mathbf{T} \in \mathbb{R}^{(8n)\times(2m+1)}$ stands for the trigonometric functions of the approximated radial function. Here $p \geq 0$ defines the corresponding Sobolev norm. Since q has to be real valued we actually solve the following regularized equation

$$\left(\mathbf{T}^\top \left(\Re(\mathbf{A})^\top \Re(\mathbf{A}) + \Im(\mathbf{A})^\top \Im(\mathbf{A})\right) \mathbf{T} + \lambda_k \mathbf{I}_p\right) \mathbf{x}$$
$$= \mathbf{T}^\top \left(\Re(\mathbf{A})^\top \Re(\mathbf{b}) + \Im(\mathbf{A})^\top \Im(\mathbf{b})\right), \quad (30)$$

on the kth step, where the matrix $\mathbf{I}_p \in \mathbb{R}^{(2m+1)\times(2m+1)}$ corresponds to the Sobolev H^p penalty term. We solve (30) using the conjugate gradient method.

We update the regularization parameter in each iteration step k by

$$\lambda_k = \lambda_0 \left(\frac{2}{3}\right)^{k-1}, \quad k = 1, 2, ...$$

for some given initial parameter $\lambda_0 > 0$. To test the stability of the iterative method against noisy data, we add also noise to the far-field patterns with respect to the L^2 norm

$$\boldsymbol{\mathcal{U}}_\delta^\infty = \boldsymbol{\mathcal{U}}^\infty + \delta \frac{\|\boldsymbol{\mathcal{U}}^\infty\|_2}{\|\boldsymbol{\mathcal{V}}\|_2} \boldsymbol{\mathcal{V}},$$
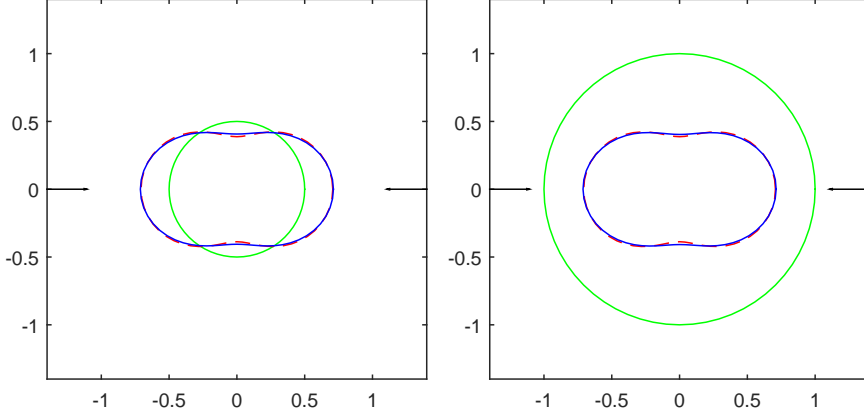
Fig. 4 Reconstruction of a peanut-shaped boundary for initial guess $r_0 = 0.5$ (left) and $r_0 = 1$ (right) and exact data.

for a given noise level δ, where $\boldsymbol{\mathcal{V}} = \boldsymbol{\mathcal{V}}_1 + i\boldsymbol{\mathcal{V}}_2$, for $\boldsymbol{\mathcal{V}}_1, \boldsymbol{\mathcal{V}}_2 \in \mathbb{R}^{8n \times 1}$ with components normally distributed random variables.

Already in the acoustic regime [2], one incident wave does not provide satisfactory results, thus we have to generalize the Iterative Scheme 1 also for multiple illuminations $\mathbf{u}_l^{inc}$, $l = 1, ..., L$.

Iterative Scheme 2 (Multiple illuminations) *Initially, we give an approximation of the radial function $r^{(0)}$. Then, in the kth iteration step:*

i. We assume that we know $r^{(k-1)}$ and we solve the L subsystems

$$\begin{pmatrix} \boldsymbol{\mathcal{A}}_1 \\ \boldsymbol{\mathcal{A}}_2 \end{pmatrix} (r^{(k-1)}; \boldsymbol{\xi}_l) + \begin{pmatrix} \boldsymbol{\mathcal{B}}_1 \\ \boldsymbol{\mathcal{B}}_2 \end{pmatrix} (r^{(k-1)}; \boldsymbol{\zeta}_l) = \begin{pmatrix} \boldsymbol{\mathcal{C}}_{1,l} \\ \boldsymbol{\mathcal{C}}_{2,l} \end{pmatrix} (r^{(k-1)}), \quad l = 1, ..., L \tag{31}$$

to obtain the densities $\boldsymbol{\xi}_l^{(k)}, \boldsymbol{\zeta}_l^{(k)}$.

ii. Then, keeping the densities fixed, we solve the overdetermined version of the linearized third equation of (22)

$$\begin{pmatrix} \boldsymbol{\mathcal{A}}_3'(r^{(k-1)}; \boldsymbol{\xi}_1^{(k)}) + \boldsymbol{\mathcal{B}}_3'(r^{(k-1)}; \boldsymbol{\zeta}_1^{(k)}) \\ \boldsymbol{\mathcal{A}}_3'(r^{(k-1)}; \boldsymbol{\xi}_2^{(k)}) + \boldsymbol{\mathcal{B}}_3'(r^{(k-1)}; \boldsymbol{\zeta}_2^{(k)}) \\ \vdots \\ \boldsymbol{\mathcal{A}}_3'(r^{(k-1)}; \boldsymbol{\xi}_L^{(k)}) + \boldsymbol{\mathcal{B}}_3'(r^{(k-1)}; \boldsymbol{\zeta}_L^{(k)}) \end{pmatrix} q =$$

$$\begin{pmatrix} \boldsymbol{\mathcal{C}}_{3,1} - \boldsymbol{\mathcal{A}}_3(r^{(k-1)}; \boldsymbol{\xi}_1^{(k)}) - \boldsymbol{\mathcal{B}}_3(r^{(k-1)}; \boldsymbol{\zeta}_1^{(k)}) \\ \boldsymbol{\mathcal{C}}_{3,2} - \boldsymbol{\mathcal{A}}_3(r^{(k-1)}; \boldsymbol{\xi}_2^{(k)}) - \boldsymbol{\mathcal{B}}_3(r^{(k-1)}; \boldsymbol{\zeta}_2^{(k)}) \\ \vdots \\ \boldsymbol{\mathcal{C}}_{3,L} - \boldsymbol{\mathcal{A}}_3(r^{(k-1)}; \boldsymbol{\xi}_L^{(k)}) - \boldsymbol{\mathcal{B}}_3(r^{(k-1)}; \boldsymbol{\zeta}_L^{(k)}) \end{pmatrix}$$
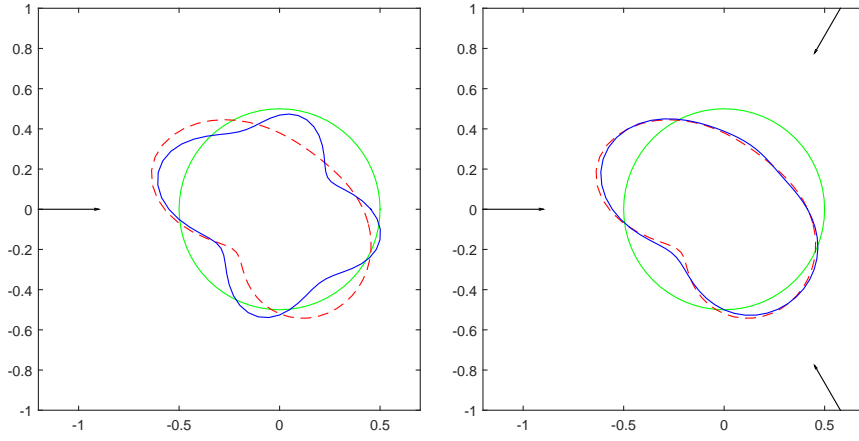
Fig. 5 Reconstruction of a apple-shaped boundary for one (left) and three (right) incident fields.
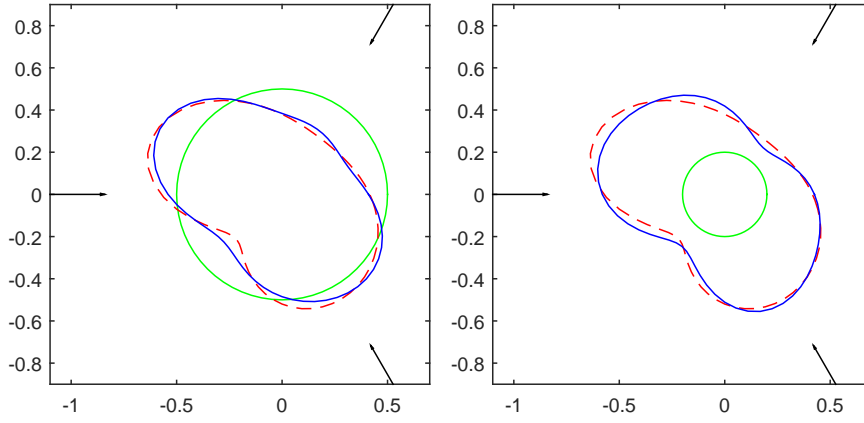

Fig. 6 Reconstruction of a apple-shaped boundary for initial guess $r_0 = 0.5$ (left) and $r_0 = 0.2$ (right) and noisy data.

for q and we update the radial function $r^{(k)} = r^{(k-1)} + q$.

The iteration stops when a suitable stopping criterion is satisfied.

6.3 Numerical results

In the following examples we choose the incident field to be a longitudinal plane wave with different incident directions given by

$$\hat{\boldsymbol{d}}_l = (\cos \tfrac{2\pi l}{L}, \sin \tfrac{2\pi l}{L}), \quad l = 1, ..., L.$$
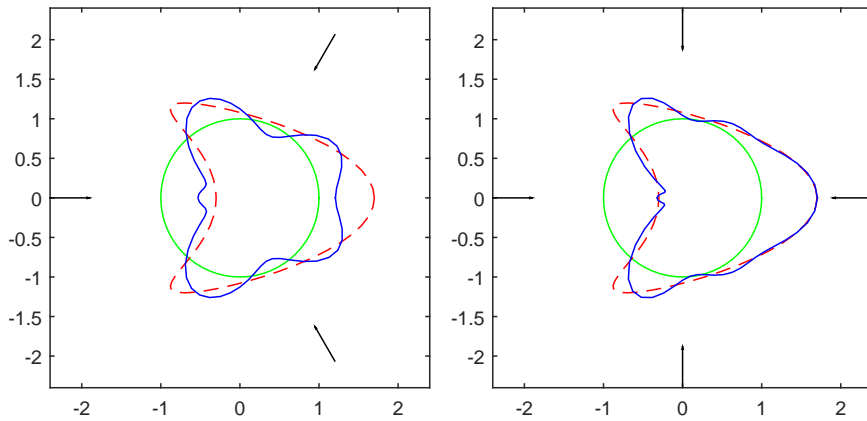
Fig. 7 Reconstruction of a kite-shaped boundary for three (left) and four (right) incident fields.

We choose the Lamé constants to be $\lambda_e = 1$, $\mu_e = 1$ and $\rho_e = 1$ in D_e and $\lambda_i = 2$, $\mu_i = 3$ and $\rho_i = 1$ in D_i and $\omega = 8$ circular frequency. We set $n = 64$ collocation points for the direct problem and $n = 32$ for the inverse. The regularized equation (30) is solved for $p = 1$, meaning H^1 penalty term and for initial regularization parameter $\lambda_0 = 0.8$.

We present reconstructions for different boundary curves, different number of incident directions and initial guesses for exact and perturbed far-field data. When, we refer to noisy data, we have considered $\delta = 5\%$. In all figures the initial guess is a circle with radius r_0, a green solid line, the exact curve is represented by a dashed red line and the reconstructed by a solid blue line. The arrows denote the directions of the incoming incident fields.

In the first example we consider the peanut-shaped boundary. The reconstructions for $m = 3$ coefficients, two incident fields and $r_0 = 0.5$ initial radius are presented in Fig. 3 after 40 iterations for the exact data and 25 iterations for the noisy. In Fig. 4, we see that the reconstructions are not highly dependent on the initial guess.

In the second example, the boundary to be reconstructed is the apple-shaped. Here, we set $m = 4$, and $r_0 = 0.5$. The reconstructions for exact data and different number of incident fields are presented in Fig. 5 for 18 iterations (one incident direction) and 40 iterations (three incident directions). Fig. 6 shows the effect of the initial guess for noisy data and 40 iterations.

In the last example, we choose the kite-shaped boundary. We consider $m = 7$ coefficients and $r_0 = 1.5$. In Fig. 7 we see the improvement with respect to the number of incident fields for exact data, 10 iterations for three illuminations and 40 iterations for four illuminations. The dependence on the initial guess is shown in Fig. 8, for $r_0 = 1$ we needed 40 iterations and 25 for $r_0 = 1.5$, in doth cases we considered noisy data.
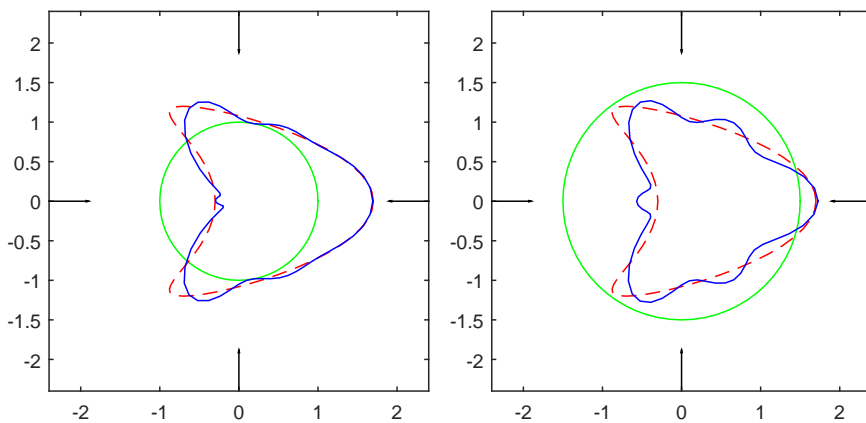
Fig. 8 Reconstruction of a kite-shaped boundary for initial guess $r_0 = 1$ (left) and $r_0 = 1.5$ (right) and noisy data.

The exponential convergence of our numerical method and the relatively small matrix size $(2m+1) \times (2m+1)$ result to fast reconstructions. In the first two examples, the time of an iteration step is less than a second, and approx. a second in the last example ($l = 4$ and $m = 7$).

All examples show the feasibility of the proposed method that is also reasonably stable against noise. The results are considerably improved if we consider more that one incident wave. One could also considered more sophisticated regularization techniques and methods to compute the regularization parameter that could improve the reconstructions but are out of the scope of this paper.

7 Conclusions

This paper addressed the problem of recovering the position of an elastic inclusion placed in a homogeneous two-dimensional elastic medium. We considered the method of boundary integral equations to transform the inverse problem to a system of integral equations. The system is non-linear with respect to the unknown boundary curve and ill-posed because of the compactness of the operator in the far-field equation. We applied an iterative scheme to solve the system of equations by linearizing only the far-field equation using the Fréchet derivatives of the far-field operators. The reconstructions were accurate for few incident waves and reasonably fast and stable.

References

1. Alessandrini, G., Morassi, A., Rosset, E.: Detecting an inclusion in an elastic body by boundary measurements. SIAM Rev. **46**(3), 477–498 (2004)

2. Altundag, A., Kress, R.: On a two-dimensional inverse scattering problem for a dielectric. Appl. Anal. **91**(4), 757–771 (2012)
3. Alves, C.J.S., Martins, N.F.M.: The direct method of fundamental solutions and the inverse kirsch-kress method for the reconstruction of elastic inclusions or cavities. J. Integral Equations Appl. **21**, 153–178 (2009)
4. Chapko, R.: On the numerical solution of a boundary value problem in the plane elasticity for a bouble-connected domain. Math. Comput. Simulat. **66**, 425–438 (2004)
5. Chapko, R., Ivanyshyn, O., Protsyuk, O.: On a nonlinear integral equation approach for the surface reconstruction in semi-infinite-layered domains. Inverse Probl. Sci. Eng. **21**(3), 547–561 (2013)
6. Chapko, R., Kress, R., Mönch, L.: On the numerical solution of a hypersingular integral equation for elastic scattering from a planar crack. IMA J. Numer. Anal. **20**, 601–619 (2000)
7. Charalambopoulos, A.: On the fréchet differentiability of boundary integral operators in the inverse elastic scattering problem. Inv. Probl. **11**, 1137–1161 (1995)
8. Charalambopoulos, A., Kirsch, A., Anagnostopoulos, K., Gintides, D., Kiriaki, K.: The factorization method in inverse elastic scattering from penetrable bodies. Inv. Probl. **23**(1), 27–51 (2007)
9. Gintides, D., Midrinos, L.: Inverse scattering problem for a rigid scatterer or a cavity in elastodynamics. ZAMM Z. Angew. Math. Mech. **91**(4), 276–287 (2011)
10. Gintides, D., Sini, M.: Identification of obstacles using only the scattered p-waves or the scattered s-wave. Inverse Probl. Imag. **6**, 39–55 (2012)
11. Hähner, P., Hsiao, G.: Uniqueness theorems in inverse obstacle scattering of elastic waves. Inv. Probl. **9**, 525–534 (1993)
12. Hu, G., Kirsch, A., Sini, M.: Some inverse problems arising from elastic scattering by rigid obstacles. Inv. Probl. **29**(1), 015009 (2013)
13. Ivanyshyn, O., Johansson, B.T.: Nonlinear integral equation methods for the reconstruction of an acoustically sound-soft obstacle. J. Integral Equations Appl. **19**(3), 289–308 (2007)
14. Ivanyshyn, O., Johansson, B.T.: Boundary integral equations for acoustical inverse sound-soft scattering. J. Inv. Ill-posed Probl. **16**(1), 65–78 (2008)
15. Ivanyshyn, O., Kress, R.: Nonlinear integral equations for solving inverse boundary value problems for inclusions and cracks. J. Integral Equations Appl. **18**(1), 13–38 (2006)
16. Johansson, B.T., Sleeman, B.: Reconstruction of an acoustically sound-soft obstacle from one incident field and the far-field pattern. IMA J. Appl. Math. **72**, 96–112 (2007)
17. Kar, M., Sini, M.: On the inverse elastic scattering by interfaces using one type of scattered waves. J. Elast. **118**(1), 15–38 (2015)
18. Knops, R. J. and Payne, L. E.: Uniqueness Theorems in Linear Elasticity. Springer, Berlin (1971)
19. Kress, R.: On the numerical solution of a hypersingular integral equation in scattering theory. J. Comput. Appl. Math. **61**(3), 345–360 (1995)
20. Kress, R.: Inverse elastic scattering from a crack. Inv. Probl. **12**, 667–684 (1996)
21. Kress, R.: Linear Integral Equations, 3 edn. Springer, New York (2014)
22. Kress, R., Rundell, W.: Nonlinear integral equations and the iterative solution for an inverse boundary value problem. Inv. Probl. **21**, 1207–1223 (2005)
23. Kupradze, V.: Three-Dimensional problems of the mathematical theory of elasticity and thermoelasticity. North-Holland Publishing Co., New York (1979)
24. Le Louër, F.: A domain derivative-based method for solving elastodynamic inverse obstacle scattering problems. Inv. Probl. **31**(11), 115006 (2015)
25. Lee, K.: Inverse scattering problem from an impedance crack via a composite method. Wave Motion **56**, 43–51 (2015)
26. Li, J., Sun, G.: A nonlinear integral equation method for the inverse scattering problem by sound-soft rough surfaces. Inverse Probl. Sci. Eng. **23**(4), 557–577 (2015)
27. Martin, P.: On the scattering of elastic waves by an elastic inclusion in two dimensions. Quart. J. Mech. and Appl. Math. **43**(3), 275–291 (1990)
28. Pelekanos, G., Kleinman, R., van den Berg, P.: Inverse scattering in elasticity a modified gradient approach. Wave Motion **32**(1), 57–65 (2000)
29. Pelekanos, G., Sevroglou, V.: Inverse scattering by penetrable objects in two-dimensional elastodynamics. J. Comput. Appl. Math. **151**(1), 129–140 (2003)

30. Qin, H.H., Cakoni, F.: Nonlinear integral equations for shape reconstruction in the inverse interior scattering problem. Inv. Probl. **27**, 035005 (2011)
31. Sevroglou, V.: The far-field operator for penetrable and absorbing obstacles in 2d inverse elastic scattering. Inv. Probl. **21**(2), 717–738 (2005)